UC Davis
UC Davis Previously Published Works

Title
Thermal transport in free-standing silicon membranes: influence of dimensional reduction and surface nanostructures

Authors
Neogi, S
Donadio, D

Peer reviewed

Thermal transport in free-standing silicon membranes: Influence of dimensional reduction and surface nanostructures

Sanghamitra Neogi and Davide Donadio

Max Planck Institute for Polymer Research, Ackermannweg 10, 55128 Mainz, Germany

Abstract. Nanostructuring provides a viable route to improve the thermoelectric performance of materials, even of those that in bulk form have very low figure of merit. This strategy would potentially enable the fabrication of thermoelectric devices based on silicon, the cheapest, most integrable and easiest to dope Earth-abundant semiconductor. A drastic reduction of the thermal conductivity, which would lead to a proportional enhancement of the figure of merit, was observed for silicon low-dimensional nanostructures, such as nanowires and ultra-thin membranes. Here we provide a detailed analysis of the phononic properties of the latter, and we show that dimensionality reduction alone is not sufficient to hinder heat transport to a great extent. In turn, the presence of surface roughness at the nanoscale reduces the thermal conductivity of sub-10 nm membranes up to 10 times with respect to bulk.

1 Introduction

The recent need for renewable energy harvesting using thermoelectric devices and for solid-state Peltier coolers to use in information and communication technology has boosted the interest towards understanding the role of lattice thermal transport in nanostructures and nanostructured materials [1,2]. Nanostructuring semiconductors was proposed as a way to improve the thermoelectric figure of merit (ZT), either by improving the electronic power factor at the numerator of ZT [3] or by reducing the thermal conductivity at the denominator, [4,5], ideally achieving a material that behaves as an electron crystal and a phonon glass [6]. In fact, control of thermal conductivity based on phonon engineering in Earth abundant and cheap materials, such as silicon, has already shown to be a promising path to viable thermoelectric (TE) devices with good performance [7,8,9,10]. A detailed understanding of phonons dispersion relations and phonon scattering in low-dimensional nanostructures can lead us to the design of materials and devices with tailored acoustic and thermal properties [11,12,7,13,14,15,16,17,18].

Recent experiments have shown a consistent reduction of the thermal conductivity of silicon thin films (silicon-on-insulator, SOI) and suspended membranes, proportional to the thinning of the silicon layer [19,20,21,22,23], with minimum thermal conductivity of 9 W/m K measured in 9 nm thick free-standing silicon membranes [23]. Correspondingly, a strong reduction of the group velocities of acoustic phonons, was observed in free-standing silicon membranes [18]. Mesoscopic models based on the theory of elasticity, which utilize the bulk properties of silicon as input parameters, fit well to the experimental results by adjusting the specularity parameter that determines

phonon surface scattering [24]. However, the applicability of mesoscopic models for sub-10 nm nanostructures is questionable and these models do not provide a clear connection between structure, phonon properties and thermal conductivity [25]. Former atomistic simulations elucidated out-of-plane thermal transport in thin films [26], but suffer from size converge issues and do not provide a reliable insight into the scattering mechanisms of in-plane phonons and their contribution to the thermal conductivity [27].

Here we provide a fully atomistic characterization of the phononic properties of silicon membranes with thickness comparable to the measured ones, performing large-scale molecular dynamics and lattice dynamics calculations. We show that dimensionality reduction modifies significantly the character of both acoustic and thermal phonons, yielding a reduction of the group velocities over the whole spectrum, with the consequence of a reduction of the thermal conductivity. Nevertheless, this effect is not sufficient to account for the experimental trends, as the thermal conductivity of our models of flat crystalline silicon membranes remains much higher than the values reported in the experiments [23]. On the other hand, we observe that models of membranes with rough surfaces yield comparable reductions of the thermal conductivity as in experiments, thus highlighting the major role played by surfaces in controlling heat transport at the nanoscale.

In the next section we review the experimental measurements on silicon membranes along with the results achieved so far by theoretical modeling. In section 3 we illustrate our atomistic models of silicon membranes. The results regarding the dispersion relations of acoustic and thermal phonons are reported in section 4, and the calculations of the thermal conductivity are reported in section 5. A brief summary and conclusions are given in section 6.

2 Thermal transport in silicon membranes and thin films

Miniaturization of electronic transistors, sensors and actuators in the late 1990s lead to the use of single-crystalline silicon layers below 0.1 μm deposited on oxide. The performances of silicon-on-insulator (SOI) fabricated devices are conditioned by the capacity of the silicon layer to dissipate heat, so to avoid overheating and possibly burn out. This development stimulated the earliest investigations on the in plane thermal conductivity (κ) of silicon thin films [19,20]. These studies, which employed harmonic Joule heating and electrical-resistance thermometry [28], showed that the thermal conductivity of silicon films with thickness in the range of 100 nm is largely reduced with respect to the bulk, due to phonon boundary scattering. The reduction of κ may exceed 50% at room temperature for 100 nm thick films [19]. Measurements also demonstrated that κ depends monotonically on the thickness of the film: the thinner the film the lower κ. The suppression of κ in films is strongly temperature dependent, especially below 200 K, i.e. for temperature regimes in which quantum effects become more prominent, indicating that the relative populations of carriers may be rather different in films than in bulk. At room temperature the thermal conductivity of SOI thin films becomes nearly indistinguishable from that of bulk for thicknesses beyond 1 μm. This trend of thermal conductivity reduction has been confirmed by measurements on even thinner single crystalline silicon films, down to 20 nm, for which $\kappa \sim 0.16\kappa_{bulk}$ was observed [29,21].

Reducing κ in SOI films would make it possible to exploit these systems for thermoelectric applications, as the Seebeck coefficient remains as large as in the bulk and can be even enhanced by doping [30,31]. However encouraging, the measurement of the thermo power of thin films indicates that room temperature thermal conductivity not larger than 2 W/m K would be necessary to achieve a thermoelectric figure of merit of 0.3, i.e. at the lower limit of thermoelectric applications. Following the pathway indicated by a pioneering atomistic modeling [32], such low values of thermal conductivity were achieved in silicon thin films with arrays of nano-holes [9,10]. In these systems a two orders of magnitude reduction of κ with respect to bulk was observed, stemming from the interplay of nanoscale morphology and atomistic disorder at hole surfaces [33].

The evidences of considerable reduction of the thermal conductivity of silicon nanowires [34,8,35,36] suggest that a possible alternative approach to reduce the thermal conductivity of crystalline silicon beyond the limits observed for SOI films, would be to fully exploit dimensionality reduction and to work with suspended two-dimensional membranes. Advances in fabrication and processing have made it possible to produce single crystalline silicon membranes as thin as 6 nm, which can be suspended in such a way to control their strain [37]. The thermal conductivity of this class of systems can be measured by Raman thermometry,[22,23] so not to interfere with phonon propagation by direct interaction of a solid probe at the
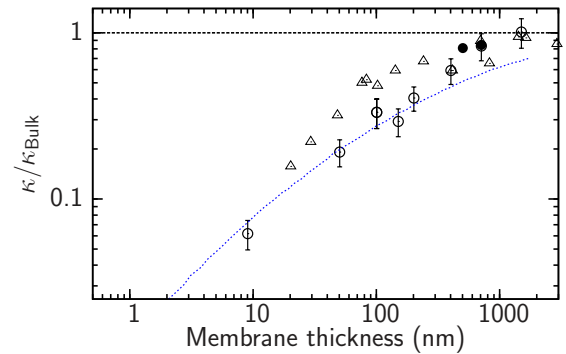

Fig. 1. Room temperature thermal conductivity of silicon thin films (triangles from Refs. [19,20,29,21]) and suspended membranes (circles from Ref. [22,23]) normalized by the thermal conductivity of natural bulk silicon (148 W/m K at 300 K) [38]. The dotted (blue) line represents the trend obtained from the mesoscopic model outlined in Ref. [24].

surface. Recent experiments resulted in a thermal conductivity of 9 W/m K at room temperature for the thinnest membrane measured so far (9 nm) [23].

Both the results on SOI thin films and on suspended membranes can be modeled using the kinetic theory of thermal diffusion, which relies on an approximated solution of the linearized Boltzmann transport equation. Using the phonon dispersion relations of bulk silicon and taking into account the different contributions from different polarization branches (z), one can express the thermal conductivity at temperature T as an integral over the phonon frequencies up to the Debye frequency (ω_D) [39]:

$$\kappa = \frac{1}{3}\sum_{z=1}^{3} v_z^2 \int_0^{\omega_D} d\omega \frac{\hbar}{k_B T} C_z(\omega)\tau_z^{bulk}(\omega)F_p(d,\omega) \quad (1)$$

where v_z is the group velocity of each acoustic branch z, $C_z(\omega)$ is the phonon specific heat per unit volume, τ_z^{bulk} the phonon lifetimes in the bulk, and F_p is a reduction function that takes into account the effect of phonon scattering at the surfaces or interfaces. F_p depends on the film thickness d and on the frequency, and rescales bulk phonon lifetimes and, consequently, phonon mean free paths. The subscript p is a specularity parameter, which ranges from 0 for purely diffusive scattering to 1 for purely specular reflection. The reduction function F_p for a two-dimensional film can be derived in analogy with the solution derived by Sondheimer for the Boltzmann equation for electronic transport [40]. Assuming fully diffusive scattering ($p = 0$) at the surfaces, this simple analytical model reproduces fairly well the thermal conductivity reduction observed for SOI films as a function of their thickness [19,20,21]. A similar model, described in detail in Ref. [24], fits well also the results for membranes [23].

Mesoscopic models can be refined introducing in the integral the complete bulk dispersion relations and relaxation times, which can be obtained by anharmonic lattice dynamics, computed either by empirical potentials [25] or by ab initio methods [41]. Using this approach and

comparing lattice dynamics results to molecular dynamics simulations Turney *et al.* showed that for film or membranes thinner than ~ 10 nm large discrepancies may arise, thus indicating that bulk dispersion relations and lifetimes cannot be used to infer the thermal conductivity of ultra-thin silicon layers, and direct atomistic simulations are necessary [25]. In addition, the use of a reduction function with a specularity parameter relies solely on phenomenological observations, and does not reveal the connection between the structure of surfaces or interfaces and the thermal conductivity of ultra-thin silicon layers either suspended or deposited on a substrate.

3 Atomistic model of silicon membranes

Microscopic configurations. Bulk crystalline silicon has a cubic diamond unit cell with an experimental lattice constant $a = 5.431$ Å. We prepared the crystalline silicon membranes by cleaving a slab from the bulk along the (001) face. We chose silicon membranes of varying thickness for our investigation: namely 0.81 nm, 1.09 nm, 3.26 nm, 5.43 nm and 10.86 nm and 20.1 nm. The (001) surface of silicon is the one used for technological application, as it does not display metallic character when it is passivated with hydrogen. To minimize the number of dangling bonds the (001) surface undergoes a 2x1 reconstruction, displaying rows of dimers [42,43,44,45]. Each atom forming a dimer has a dangling bond that can be passivated by hydrogen. Such 2x1 reconstruction is energetically favourable and is stable at high temperature. Former tests on thin silicon nanowires showed that including explicit hydrogens in the MD simulations would not alter the resulting thermal conductivity, which may be very sensitive to surface disorder [46]. Side views of representative microscopic configurations of 1 and 5 nm-thick membranes, and a top view displaying the surface reconstruction are shown in Figure 2. We also consider models of membranes with a periodic surface roughness, with 1 nm thick features modulating the surface with a correlation length of about 2 nm.

Interatomic potential. In order to compute the interatomic forces in our atomistic model systems, we used empirical potentials, which are parametrised by fitting to fundamental properties of bulk silicon, such as the elastic constants, the equilibrium volume, the binding energy or the formation energy of point defects. The choice of empirical interatomic potentials is dictated by the necessity to calculate the phonon properties and the thermal conductivity of models in the same range of thickness as the experiments. We can thus perform molecular dynamics simulations of systems of up to ten millions of atoms for several nanoseconds, so to get well converged estimates of the thermal conductivity of membranes up to 20 nm thick. For covalently bonded solids, such as silicon and germanium, different empirical potentials were proposed: Stillinger-Weber [47], environment dependent interatomic potential (EDIP) [48] and Tersoff bond-order potential
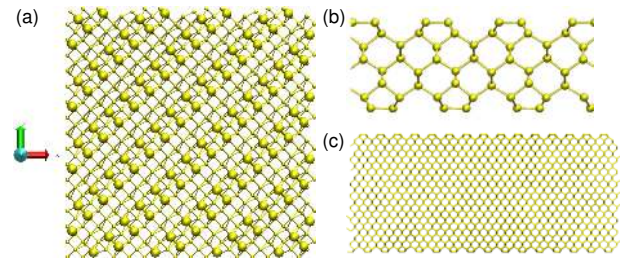

Fig. 2. (a) Top view of 1nm-thick silicon membrane. The top surface atoms are marked with larger spheres to illustrate the row of dimers at the surface. Side views of (b) 1 nm-thick and (c) 5 nm-thick membranes to illustrate reconstructed surfaces: surface reconstruction is visible by the presence of dimers at the surface, especially for the 1 nm-thick membrane. The red and green arrows indicate the crystallographic directions along which the phonon dispersions are calculated.

[49]. The Tersoff potential has been used to study surface reconstructions [50] and with results consistent with experiments [51]. In addition the Tersoff potential can accurately describe the properties of non-tetrahedral forms of silicon and provides a good representation of the phonon dispersion relation of bulk silicon (Fig. 3a). For these reasons we chose the Tersoff empirical potential [49] for our study.

4 Phonon properties of suspended silicon membranes

Phonon bands engineering in nanostructures has gained an increasing attention in recent years [15,18], especially with the intent of designing of thermoelectric systems with improved efficiency [52]. In suspended membranes thickness is the main control parameter. We computed the phonon dispersions of silicon membranes with 2×1 reconstructed surfaces as a function of thickness using harmonic lattice dynamics. The dispersion relations are computed by direct diagonalisation of the dynamical matrix of a unit cell of the actual slab geometry and Fourier expansion along the symmetry directions of the two-dimensional Brillouin zone.

Figure 3 (b) shows the phonon dispersion relations of crystalline silicon membrane of thickness 5.43 nm to be compared to the bulk dispersion relations shown in Figure 3 (a). The range of frequencies of the longitudinal acoustic (LA) and transverse acoustic (TA) modes is reduced with respect to the bulk, and a large number of higher-order flexural or breathing modes appears. The thinner the membranes the smaller the range of acoustic frequencies, indicating an average softening of the elastic moduli, especially for the out-of-plane components. On the other hand the number of higher-order modes increases with thickness, as a consequence of the increasing number of atoms in the unit cell.

Figure 3 (c) zooms into the dispersion relations of the three fundamental acoustic branches of the membranes of
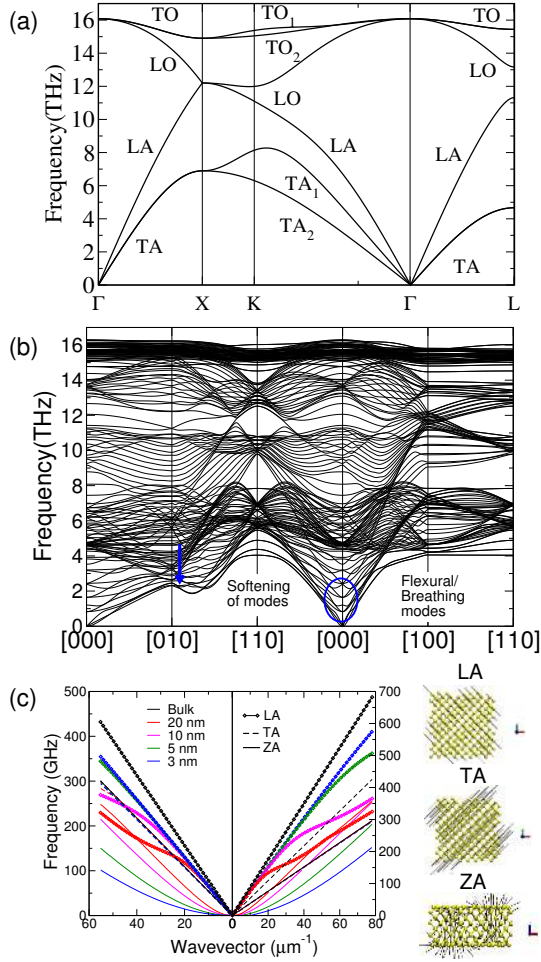
Fig. 3. (a) Phonon dispersion in bulk silicon. (b) Phonon dispersion in 3 nm-thick silicon membrane along different symmetry directions. The softening of modes in general and the presence of out-of-plane ZA modes can be clearly discerned. (c) Phonon dispersion for small values of wavevectors in silicon membranes of different thicknesses in comparison with bulk. The ZA modes are mostly affected by the membrane thickness.

Fig. 4. (a) Phonon group velocities in free-standing silicon membranes compared to bulk. Phonon group velocities are reduced in the 5 nm-thick membrane and decrease in reducing the membrane thickness.

Fig. 5. Speed of sound in silicon membranes as a function of thickness. The speeds of sound of LA modes are reduced in the membranes.

thicknesses 3 nm (blue), 5 nm (green), 10 nm (magenta) and 20 nm (red), in comparison to bulk (black), near the Γ point. The lowest frequency modes, compatible with the periodicity of a membrane supercell containing ~ 5000 atoms, with LA, TA and ZA polarisation are displayed in the snapshots in Figure 3 (c), in which the atomic displacements are represented by grey lines. Displacement vectors were obtained by diagonalising the dynamical matrix of the supercell. The LA modes of the membranes are slightly flattened as compared to bulk, while one of the TA modes remains unchanged. The most prominent effect of dimensionality reduction is the lifting of the degeneracy of the TA modes and the conversion of one of the TA modes into a flexural out-of-plane modes (ZA), with quadratic dispersion relation at zone centre. These ZA modes are very sensitive to the reduction of the membrane t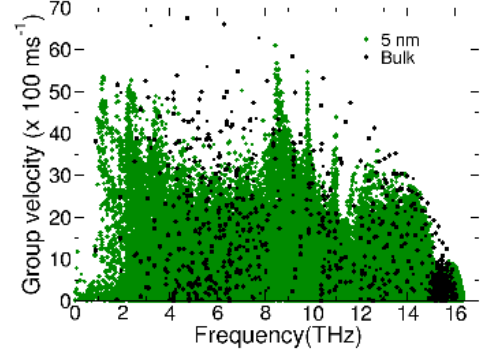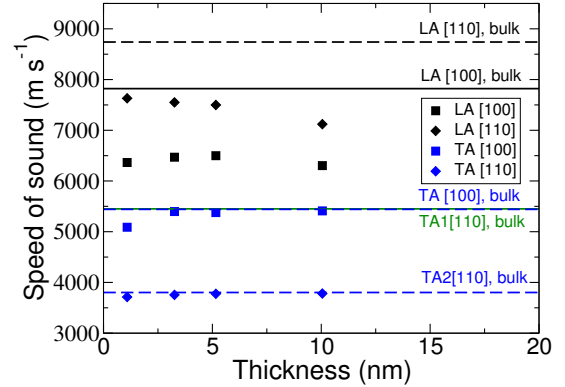hickness, and gets softer the thinner the membranes. This effect, observed by Brillouin light scattering measurements [18], pinpoints the need to explicitly consider the modified dispersion relations in low-dimensional structures. Such softening of the ZA modes can also be predicted using the theory of elasticity for Lamb's waves [53].

The slope of the phonon dispersion curves at the Γ point gives the speed of sound for each polarization branch. Figure 5 shows the speed of sound longitudinal, and transverse modes as a function of membrane thickness for (100) and (110) propagation directions. The speed of sound of the longitudinal modes is reduced compared to that in the bulk crystalline silicon, whereas the speed of sound of the transverse mode remain almost unaltered (see also Figure 3(c)). Note that there is only one transverse TA mode in the membranes, as the other one is converted into a flexural ZA mode, which has zero group velocity at the Γ point.

Even though they provide valuable information on the acoustic and elastic properties of the system, phonons in the GHz regime do not affect significantly thermal conductivity, which is mostly determined by the features of
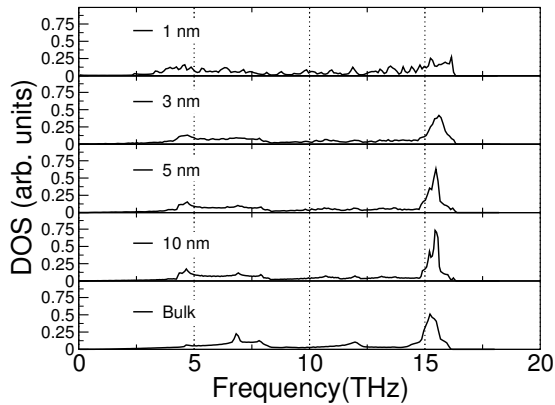
Fig. 6. Vibrational density of states in silicon membranes of different thickness. The population of the phonon modes in the membranes is increased in the low frequency region.

phonons in the THz regime. In this range of frequencies dimensionality reduction leads to an overall flattening of the phonon dispersions, resulting in lower phonon group velocities, which are computed as the gradient of the frequency (ω) with respect to the wavevector $\mathbf{q}$, i.e. $v_g(\omega) = \partial\omega(\mathbf{q})/\partial\mathbf{q}$.

In a bulk material, the thermal conductivity tensor can be expressed as [54]

$$\kappa_{\alpha\beta} = \sum_{\mathbf{q},z} c_{\mathrm{ph},\lambda}(\mathbf{q}) v_{z,\alpha} v_{z,\beta}(\mathbf{q}) \tau_z(\mathbf{q}) \tag{2}$$

where, $\mathbf{q}$ and z are the phonon wavevector and polarization, $c_{\mathrm{ph},z}(\mathbf{q})$ is the phonon specific heat per unit volume, $v_{z,\alpha}(\mathbf{q})$ is the component of phonon group velocity vector along the Cartesian direction α, and $\tau_z(\mathbf{q})$ is the phonon lifetime. The phonon group velocity term has thus a dominant role in the thermal conductivity expression and hence, can help us to make a qualitative prediction about the thermal conductivities in the material. In Figure 4, we show the phonon group velocities in silicon membranes of thicknesses 5 nm (green), along with the phonon group velocities in bulk silicon (black). The phonon group velocities are reduced in the membranes compared to bulk, especially in the low frequency region, which plays a dominating role in thermal transport. Dimensionality reduction is therefore expected to lower the thermal conductivity of silicon membranes as expressed in Eq. 2, through the observed reduction of the group velocities of acoustic phonons.

The sum in Eq. 2 is implicitly affected by the vibrational density of states (VDOS) of the system, which is also a function of the membrane thickness. In order to obtain the phonon vibrational density of states (VDOS) in the crystalline silicon membranes, we have integrated the first Brillouin zone using a 40×40 Monkhorst–Pack mesh of q- points [55]. The VDOSs are reported in Figure 6 for crystalline silicon membranes of 1 nm, 3 nm, 5 nm and 10 nm thickness. The bulk VDOS is also given for reference. We observe a shift towards lower frequencies of the bulk acoustic band between 5 and 8 THz. This

shift results in the appearance of a peak below 5 THz in the membranes, which which broadens and shifts toward lower frequencies in the thinnest ones (1 and 3 nm). In turn, the intensity of the peak related to optical modes at about 16 THz decreases with decreasing thickness of the membranes. For the 1 nm membrane, the sharp optical peak is largely reduced and broadened toward lower frequencies. Although the phonon density of states is higher in the low frequency (~ 5 THz) region in the membranes, they would not contribute greatly to thermal conductivity because of the lowered group velocities.

5 Thermal transport in free-standing silicon membranes

5.1 Molecular dynamics

The harmonic lattice dynamics calculations presented in the previous section are not sufficient to assess quantitatively the thermal conductivity of membranes. We then used classical molecular dynamics (MD) to compute the thermal conductivity in the crystalline silicon membranes. There are two possible approaches to calculate the thermal conductivity of a system by MD simulations. The first approach is to perform equilibrium MD (EMD) simulations and obtain the thermal conductivity from the autocorrelation function of the heat current using the fluctuation-dissipation theorem and the respective Green-Kubo relation [56]. The second approach is to perform non-equilibrium MD (NEMD) simulations and calculate the thermal conductivity using Fourier's heat equation [57,58,59,60]. The NEMD approach, though more intuitive, requires a careful size-scaling analysis extrapolate to bulk thermal conductivities. Such extrapolation is often far from trivial [61]. NEMD was used in the past to compute thermal transport in silicon membranes, but the results were not conclusive as size scaling analysis was not performed [27].

Here we employ the EMD method. In EMD simulations the diagonal components of the thermal conductivity can be written as [56]:

$$\kappa_{\alpha\alpha} = \frac{1}{k_B V T^2} \int_0^\infty \mathrm{d}t \langle J_\alpha(t) J_\alpha(0) \rangle \tag{3}$$

where $\alpha = x, y, z$; k_{B} is the Boltzmann constant, V is the volume of the system, T is the temperature, and $\langle J_\alpha(t) J_\alpha(0) \rangle$ is the heat current autocorrelation function along the direction (α) of heat propagation. The heat current is given by:

$$\mathbf{J} = \sum_i^N \epsilon_i \mathbf{v}_i + \frac{1}{2} \sum_{i,j;i\neq j}^N (\mathbf{F}_{ij} \cdot \mathbf{v_i}) \mathbf{r}_{ij} + $$
$$\frac{1}{6} \sum_{i,j,k;i\neq j\neq k}^N (\mathbf{F}_{ijk} \cdot \mathbf{v_i})(\mathbf{r}_{ij} + \mathbf{r}_{ik}), \tag{4}$$

where ϵ_i and $\mathbf{v}_i$ are the energy density and velocity associated with atom i, respectively. $\mathbf{F}$ represents the in-

teratomic force acting between atoms separated by a distance $\mathbf{r}$. A disadvantage of this approach is that the convergence of the heat current autocorrelation function can be very slow, requiring long MD runs (several tens of ns for silicon-based materials), however in general size convergence is achieved more easily than for NEMD and no extrapolation is required [58,62]. Our calculations of the in-plane $(x - y)$ thermal conductivity of crystalline silicon membranes by EMD simulations are performed using the LAMMPS package [63]. We applied periodic boundary conditions in the x and y directions, thus mimicking the simulation of an infinite plane, and the simulation supercell is built in such a way that periodic images of the slab do not interact in the perpendicular direction (z-direction). The volume of the system is defined as the product of the area of the $x - y$ plane of the cell times the membrane thickness. We use a time step of 1 fs for our simulations to calculate the thermal conductivities of the smooth membranes. The systems employed in the MD simulations were constructed replicating the unit cells of silicon membranes described in the first subsection. We chose five samples of silicon membranes of various thicknesses for our investigation: namely 1.09 nm, 3.26 nm, 5.43 nm and 10.86 nm and 20.1 nm.

Each sample was equilibrated using the Nosé-Hoover thermostat [64] set at 300 K for 100 ps, while the surface area in the x,y plane was kept constant. The system was then coupled to a barostat set at zero pressure and was allowed to expand or contract the volume in order to obtain unstrained configurations. This step was performed for times of the order of 1 ns. After equilibration, the velocities were set to 300 K and the systems were again coupled to a Nosé-Hoover thermostat for 1 ns to decorrelate the systems from the initial configurations. The thermostat was then decoupled from the systems and the heat flux calculations were performed under microcanonical conditions (constant number of particles N, volume V, and energy E) using Eq. 4, and recorded every 5 fs intervals. The thermal conductivities were calculated using the Green-Kubo formula Eq. 3.

We have tested the convergence of κ of crystalline silicon membrane as a function of simulation time. Our results showed that simulations of the order of 20 ns are necessary to obtain a converged value of κ. We also tested the convergence of κ with respect to the truncation time used in the integration of the heat current autocorrelation function $\langle J_\alpha(t)J_\alpha(0)\rangle$ in Eq. 3. A truncation time of 200 ps yielded well-converged values for κ of Si membranes. In order to test size effects, we carried out simulations with the $\Delta t = 1$ nm-thick membrane for supercells of various sizes, starting from $4 \times 4 \times \Delta t$ nm^3 up to $32 \times 32 \times \Delta t$ nm^3, here Δt is the thickness of the sample in nm. In Fig. 7, we show the κ values for crystalline silicon membranes of thickness 1 nm as a function of the number of atoms in the simulation cell. We find that to obtain a converged value of κ of the silicon membranes under consideration, one has to use cells at least of dimension $8 \times 8 \times \Delta t$ nm^3. As shown in Fig. 7, the calculated values of κ using super-
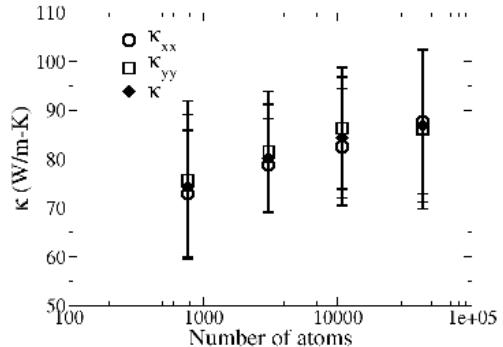

Fig. 7. Thermal conductivity in crystalline silicon membrane of 1 nm thickness as a function of the number of atoms in the simulation cell at $T = 300$K, computed with EMD, using the GreenKubo formula. The four data points represent four different samples: $4 \times 4 \times \Delta t$ nm^3, $8 \times 8 \times \Delta t$, $16 \times 16 \times \Delta t$ nm^3 and $32 \times 32 \times \Delta t$ nm^3, respectively. The final converged value of κ for crystalline silicon membrane of thickness 1 nm is given by 73.5 ± 8.9 W/m-K.
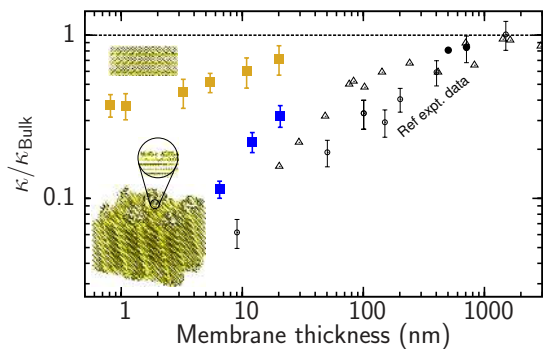

Fig. 8. Normalized thermal conductivities ($\kappa/\kappa_{\text{bulk}}$) of silicon membranes at $T = 300$K as a function of membrane thickness. The filled squares represent results from EMD simulations computed using the Green-Kubo relation: yellow squares represent crystalline membranes with 2×1 surface reconstruction. The blue squares represent nanopatterned crystalline membranes with 1 nm-high silicon nanocolumns at the surface respectively. The black circles (open and closed) and the black diamonds in the shaded area represent experimental data on silicon membranes [22,23] and SOI thin films [19,65,20,66], respectively.

cells with $8 \times 8 \times \Delta t$, $16 \times 16 \times \Delta t$ nm^3 and $32 \times 32 \times \Delta t$ nm^3 are the same within error bars.

The thermal conductivities at temperature $T = 300$K in crystalline silicon membranes as a function of membrane thickness is reported in Figure 8 (orange squares). Each of the κ values reported in Fig. 8 was obtained averaging over between 10 and 20 calculations performed starting from independent initial conditions, and the standard error is reported as the uncertainty. The reduced κ values are reported with respect to κ_{bulk} of bulk crystalline silicon computing using the same approach, 197 ± 20

W/m-K [62]. We note that the theoretical reference value for κ_{bulk} is overestimated with respect to the experimental 160 W/m-K, obtained for isotopically enriched silicon [67], due to shortcomings of the empirical forcefield. As can be seen from the figure, the thermal conductivity of crystalline silicon membranes decreases with decreasing thickness. A maximum of 3-fold reduction is obtained for the 1 nm-thick membrane, although the values lie well above the experimental results. Thermal conductivities increase toward the bulk value as we increase the thickness of the membranes as expected, but for the 20 nm thick membrane we still observe a reduction of about 25% with respect to κ_{bulk}. These results, in clear qualitative disagreement with the experiments, provide an estimate of how much phonon engineering by dimensionality reduction alone can affect the thermal conductivity of silicon. It is then clear that further sources of phonon scattering must be present in the crystalline membranes or thin films measures experimentally.

5.2 Nanostructured silicon membranes

The surfaces of the crystalline silicon membranes do not remain smooth during fabrication and processing but present atomic scale roughness. To model a more realistic silicon membrane, we introduce nanostructures at the surfaces of the smooth membranes. Moreover, nanostructuring is a viable and efficient way to control the phonon properties of materials and thermal transport. Our approach is to investigate the thermal conductivities in Si-membranes with nanopatterned surfaces that trigger local resonances. The inclusion of local resonators is fairly advantageous since the local resonances can be tuned to the underlying phonon dispersion of the crystalline material so that the thermal conductivity is reduced [68].

The microscopic configuration of the nanostructured Si-membrane we investigated is shown in the inset in Fig. 8. The silicon membrane surfaces are decorated with a periodic array of nanocolumns. We consider crystalline membranes with thickness of 5 nm, 10 nm and 20 nm, respectively. The nanocolumns on the surfaces are 2×2 nm^2 in area and 1 nm in height. We prepared the nanopatterned membrane samples by cutting from bulk of silicon. The samples are annealed by heating the sample to 1500 K and then quenching it to 300 K with a cooling rate of $\sim 10^{11}$ Ks^{-1} using a Langevin thermostat. The thermal conductivities in the nanostructured silicon membranes were calculated from EMD simulations carried out in the NVE ensemble using the Green-Kubo formula Eq. 3. We use a time step of 0.5 fs so to guarantee energy conservation over simulation times of several tens of ns. The total simulation runtime is 20 ns and we use a truncation time of 100-200 ps.

In Fig. 8, we show the reduced thermal conductivities at temperature T=300K of nanostructured crystalline silicon membranes as a function of membrane thickness (blue squares). The reduced κ values are computed with respect to $\kappa_{bulk} = 196.8 \pm 20$ W/m-K [62]. The κ values shown in the figure are the averages of 10 or more different sample
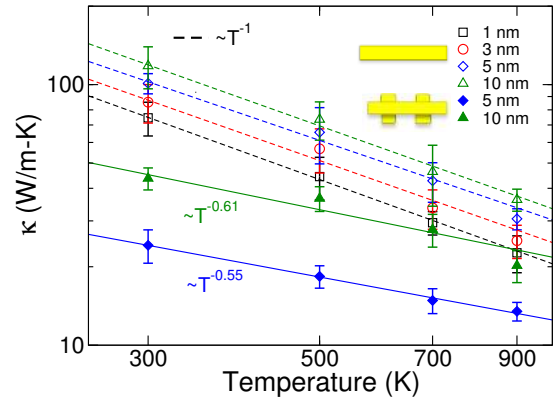

Fig. 9. Temperature dependences of thermal conductivities (reduced with respect to the bulk crystalline silicon) in crystalline silicon membranes. We considered four membranes with thicknesses: 1nm (green squares), 3 nm (blue circles), 5 nm (red diamonds) and 10 nm (black triangles), and 5 and 10 nm thick membranes with rough surfaces (filled symbols). The dashed lines represent the fitting with a function A/T^{α}. α is about 1 for crystalline membranes and < 1 for those with nanoscale surface roughness.

runs with randomly chosen initial velocities. The thermal conductivity of crystalline Si membranes decreases with the introduction of resonating nanopatterns at the two free surfaces. The reduction of the thermal conductivities is more pronounced for thinner membranes, which have a larger surface-to-bulk ratio, reaching a 10-fold reduction for the 5 nm thick nanopatterned membrane. It is worth noting that even though the simulated κ values lie above the experimental measurements, nanostructuring is quite efficient in reducing the thermal conductivity of silicon membranes.

5.3 Temperature dependence of thermal conductivities

In order to investigate the effect of temperatures on the thermal transport properties in the crystalline silicon membranes, we carried out simulations on silicon membranes at different temperatures $T = 300K$, $T = 500K$, $T = 700K$, $T = 900K$. We needed to use a time step of 0.5 fs for the EMD simulations performed at $T = 500K$, $T = 700K$, $T = 900K$ so that the total energy is conserved during the total duration of the simulation with the NVE ensemble. We ran the simulations for a total of 20 ns and use a truncation time of the order of 100-200 ps. In Fig. 9, we show the thermal conductivities of crystalline silicon membranes of four different thicknesses 1, 3, 5 and 10 nm, as a function of temperature. The points in the graph were fitted with a power-law function and the exponents were found to be in the range of -1.05 to -1. The inverse proportionality between κ and temperature implies that anharmonic phonon-phonon scattering is the only mechanism that limits heat transport in crystalline silicon membranes. The same quantity $\kappa(T)$ for rough membranes decays as $1/T^{\alpha}$, with $\alpha < 1$, indicating that temperature-

independent surface scattering takes over phonon-phonon scattering in controlling the thermal conductivity of the membranes. Similar trends were observed in thin silicon nanowires upon surface amorphization [69].

6 Conclusions

In summary, we computed the phonon properties and the thermal conductivity of Si membranes with thickness ranging from 1 nm to 20 nm by atomistic methods. The effect of dimensional reduction can be distinguished in the phonon dispersion in the crystalline Si membranes by the flattening of phonon bands and the appearance of flexural or breathing modes. The flattening of phonon bands leads to a reduction in the phonon group velocities and consequently, up to a 3-fold reduction in thermal conductivities in crystalline Si membranes. The insertion of nanopatterns at the silicon membrane surface significantly effects the thermal transport properties of the membranes. The thermal conductivity decreases with the insertion of nanopatterns. The reduction in the thermal conductivities is more pronounced for nanopatterned surfaces with a larger surface-to-bulk ratio. A 10-fold reduction of κ is observed upon nano-patterning of the surfaces. Thermal conductivity in the crystalized Si membranes is proportional to $1T$, while the temperature decay of κ is slower for nanopatterned membranes. This implies that phonon-phonon scattering is the only scattering mechanism in crystalline Si membranes, while surface scattering plays a significant role in the thermal transport in nanopatterned silicon membranes.

Acknowledgements

References

1. A. Majumdar, Science **303**, 777 (2004).
2. A. Majumdar, Nature Nanotechnology **4**, 214 (2009).
3. L. D. Hicks and M. S. Dresselhaus, Phys Rev B **47**, 16631 (1993).
4. A. Balandin, Phys. Low-Dimens. Str. **1–2**, 1 (2000).
5. J.-H. Lee, G. A. Galli, and J. C. Grossman, Nano Lett. **8**, 3750 (2008).
6. G. J. Snyder and E. S. Toberer, Nat. Mater. **7**, 105 (2008).
7. M. S. Dresselhaus *et al.*, Adv. Mater. **19**, 1043 (2007).
8. A. I. Boukai *et al.*, Nature **451**, 168 (2008).
9. J.-K. Yu *et al.*, Nat. Nanotechnol. **5**, 718 (2010).
10. J. Tang *et al.*, Nano Lett **10**, 4279 (2010).
11. A. Balandin and K. L. Wang, Phys. Rev. B **58**, 1544 (1998).
12. G. Chen, Int. J. Therm. Sci. **39**, 471 (2000).
13. G. Chen, J. Nanopart. Res. **2**, 199 (2000).
14. G. Chen, A. Narayanaswamy, and C. Dames, Superlattice Microst. **35**, 161 (2004).
15. A. A. Balandin, J. Nanosci. Nanotechnol. **5**, 1015 (2005).
16. C. J. Vineis, A. Shakouri, A. Majumdar, and M. G. Kanatzidis, Adv. Mater. **22**, 3970 (2010).
17. J.-F. Li, W.-S. Liu, L.-D. Zhao, and M. Zhou, NPG Asia Mater. **2**, 152 (2010).
18. J. Cuffe *et al.*, Nano Lett. **12**, 3569 (2012).
19. M. Asheghi, Y. K. Leung, S. S. Wong, and K. E. Goodson, Appl Phys Lett **71**, 1798 (1997).
20. Y. S. Ju and K. E. Goodson, Appl Phys Lett **74**, 3005 (1999).
21. W. Liu and M. Asheghi, J Appl Phys **98**, 123523 (2005).
22. X. Liu, X. Wu, and T. Ren, Appl Phys Lett **98**, 174104 (2011).
23. E. Chávez-Ángel *et al.*, APL Mater. **2**, 012113 (2014).
24. J. A. Johnson *et al.*, Phys. Rev. Lett. **110**, 025901 (2013).
25. J. E. Turney, A. J. H. McGaughey, and C. H. Amon, J. Appl. Phys. **107**, 024317 (2010).
26. C. J. Gomes, M. Madrid, J. V. Goicochea, and C. H. Amon, iIn-plane and Out-of-plane Thermal Conductivity of Silicon Thin Films Predicted by Molecular Dynamics, 2006.
27. P. Heino, Eur. Phys. J. B **60**, 171 (2007).
28. Y. S. Ju, K. Kurabayashi, and K. E. Goodson, Thin Solid Films **339**, 160 (1999).
29. W. Liu and M. Asheghi, Appl Phys Lett **84**, 3819 (2004).
30. C. N. Liao, C. Chen, and K. N. Tu, J Appl Phys **86**, 3204 (1999).
31. H. Ikeda and F. Salleh, Appl Phys Lett **96**, 012106 (2010).
32. J. H. Lee, J. C. Grossman, J. Reed, and G. Galli, Appl Phys Lett **91**, 223110 (2007).
33. Y. He *et al.*, ACS Nano **5**, 1839 (2011).
34. D. Li *et al.*, Appl Phys Lett **83**, 2934 (2003).
35. R. Chen *et al.*, Phys. Rev. Lett. **101**, 105501 (2008).
36. K. Hippalgaonkar *et al.*, Nano Lett **10**, 4341 (2010).
37. A. Shchepetov *et al.*, Appl. Phys. Lett. **102**, 192108 (2013).
38. C. J. Glassbrenner and G. A. Slack, Phys. Rev. **134**, A1058 (1964).
39. M. G. Holland, Phys Rev **132**, 2461 (1963).
40. E. H. Sondheimer, Advances in Physics **1**, 1 (1952).
41. D. A. Broido *et al.*, Appl Phys Lett **91**, 231922 (2007).
42. J. A. Appelbaum, G. A. Baraff, and D. R. Hamann, Phys. Rev. B **14**, 588 (1976).
43. D. J. Chadi, Phys. Rev. Lett. **43**, 43 (1979).
44. J. E. Northrup, Phys. Rev. Lett. **54**, 815 (1985).
45. P. C. Weakliem and E. A. Carter, J. Chem. Phys **96**, 3240 (1992).
46. D. Donadio and G. Galli, Phys. Rev. Lett. **102**, 195901 (2009).
47. F. H. Stillinger and T. A. Weber, Phys Rev B **31**, 5262 (1985).
48. M. Z. Bazant and E. Kaxiras, Phys. Rev. Lett. **77**, 4370 (1996).
49. J. Tersoff, Phys Rev B **39**, 5566 (1989).
50. P. C. Kelires and J. Tersoff, Phys. Rev. Lett. **63**, 1164 (1989).
51. K. L. Whiteaker, I. K. Robinson, J. E. Van Nostrand, and D. G. Cahill, Phys Rev B **57**, 12410 (1998).
52. G. Pernot *et al.*, Nature Mater. **9**, 491 (2010).
53. L. P. Solie and B. A. Auld, J. Acoust. Soc. Am. **54**, 50 (1973).

54. J. M. Ziman, *Electrons and phonons: the theory of transport phenomena in solids* (Clarendon Press, Oxford, UK, 2001).
55. H. J. Monkhorst and J. D. Pack, Phys Rev B **13**, 5188 (1976).
56. R. Zwanzig, Annu. Rev. Phys. Chem. **16**, 67 (1965).
57. F. Müller-Plathe, The Journal of chemical physics **106**, 6082 (1997).
58. P. Schelling, S. Phillpot, and P. Keblinski, Phys. Rev. B **65**, 144306 (2002).
59. E. Lampin, Q.-H. Nguyen, P. Francioso, and F. Cleri, Appl Phys Lett **100**, 131906 (2012).
60. C. Melis, R. Dettori, S. Vandermeulen, and L. Colombo, Eur. Phys. J. B **87**, 96 (2014).
61. D. P. Sellan *et al.*, Phys Rev B **81**, 214305 (2010).
62. Y. He, I. Savic, D. Donadio, and G. Galli, Phys. Chem. Chem. Phys. **14**, 16209 (2012).
63. S. Plimpton, J. Comput. Phys. **117**, 1 (1995).
64. S. Nosé, J. Chem. Phys. **81**, 511 (1984).
65. M. Asheghi *et al.*, J. Heat Transfer **120**, 30 (1998).
66. W. Liu and M. Asheghi, J. Appl. Phys. **98**, 123523 (2005).
67. R. Kremer *et al.*, Solid State Commun **131**, 499 (2004).
68. B. L. Davis and M. I. Hussein, Phys. Rev. Lett. **112**, 055505 (2014).
69. D. Donadio and G. Galli, Nano Lett **10**, 847 (2010).